Contents lists available at ScienceDirect

# Science of the Total Environment

journal homepage: www.elsevier.com/locate/scitotenv



# GO-CeO<sub>2</sub> nanohybrid for ultra-rapid fluoride removal from drinking water



Umma S. Rashid <sup>a,1</sup>, Tonoy K. Das <sup>a,1</sup>, Tamil S. Sakthivel <sup>b</sup>, Sudipta Seal <sup>b,c,\*</sup>, Achintya N. Bezbaruah <sup>a,\*\*</sup>

- <sup>a</sup> Nanoenvirology Research Group, Department of Civil and Environmental Engineering, North Dakota State University, Fargo, ND 58105, USA
- b Advanced Materials Processing and Analysis Center (AMPAC), Nanoscience and Technology Center (NSTC), Materials Science and Engineering (MSE), University of Central Florida, Orlando, USA
- <sup>c</sup> College of Medicine, University of Central Florida, Orlando, FL 32826, USA

#### HIGHLIGHTS

# Graphene oxide-ceria (GO-CeO<sub>2</sub>) nanohybrid exhibited ultra-rapid kinetics (<1 min) for F<sup>-</sup> removal.

- Maximum F<sup>-</sup> adsorption capacity was 8.61 mg/g at pH 6.5 and 16.07 mg/g at pH 4.0.
- Both electrostatic interaction and surface complexation participated in the F<sup>-</sup> removal process.
- The nanohybrid has the potential for use in high throughput defluoridation systems.

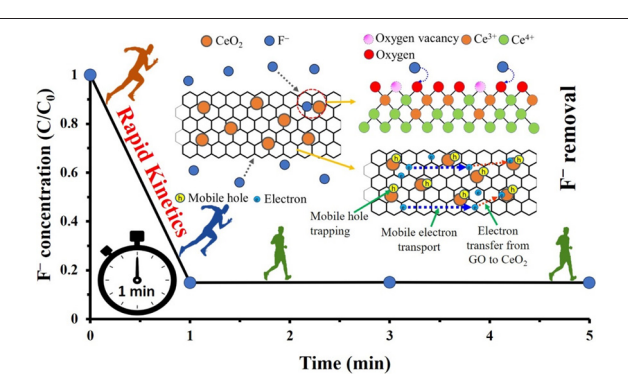
#### ARTICLE INFO

Article history: Received 18 March 2021 Received in revised form 6 June 2021 Accepted 15 June 2021 Available online 19 June 2021

Editor: Baoliang Chen

Keywords: Graphene oxide Ceria Fluoride Adsorption Rapid kinetics Nanohybrid

#### GRAPHICAL ABSTRACT



#### ABSTRACT

The presence of excess fluoride ( $F^- > 1.5 \text{ mg/L}$ ) in drinking water affects more than 260 million people globally and leads to dental and skeletal fluorosis among other health problems. This study investigated fluoride removal by graphene oxide-ceria nanohybrid ( $GO-CeO_2$ ) and elucidated the mechanisms involved. The nanohybrid exhibited ultra-rapid kinetics for fluoride removal and the equilibrium (85% removal, 10 mg  $F^-/L$  initial concentration) was achieved within 1 min which is one of the fastest kinetics for fluoride removal reported so far. Fluoride removal by the nanohybrid followed Langmuir isotherm with a maximum adsorption capacity of 8.61 mg/g at pH 6.5 and that increased to 16.07 mg/g when the pH was lowered to 4.0. Based on the experimental results and characterization data, we have postulated that both electrostatic interaction and surface complexation participated in the fluoride removal process. The  $O^{2-}$  ions present in the  $CeO_2$  lattice were replaced by  $F^-$  ions to make a coordination compound (complex). While both  $Ce^{4+}$  and  $Ce^{3+}$  were present in ceria nanoparticles ( $CeO_2$  NPs),  $Ce^{3+}$  participated in fluoride complexation. During fluoride removal by  $GO-CeO_2$ , the GO sheets acted as electron mediators and help to reduce  $Ce^{4+}$  to  $Ce^{3+}$  at the  $CeO_2$  NPs-GO interface, and the additional  $Ce^{3+}$  enhanced fluoride removal by the nanohybrid.

© 2021 Elsevier B.V. All rights reserved.

<sup>\*</sup> Correspondence to: S. Seal, Advanced Materials Processing and Analysis Center (AMPAC), Nanoscience and Technology Center (NSTC), Materials Science and Engineering (MSE), University of Central Florida, Orlando, USA.

<sup>\*\*</sup> Correspondence to: A.N. Bezbaruah, Nanoenvirology Research Group, Civil and Environmental Engineering Department, North Dakota State Univerity, Fargo, USA. E-mail addresses: sudipta.seal@ucf.edu (S. Seal). a.bezbaruah@ndsu.edu (A.N. Bezbaruah).

<sup>&</sup>lt;sup>1</sup> Joint first authors. Both the authors contributed equally to the conceptualization, design, experimentation, data collection and interpretation, and manuscript writing.

#### 1. Introduction

Fluoride (F<sup>-</sup>) is an essential trace element necessary for human teeth and skeletal health (Chouhan and Flora, 2010). However, excessive intake of fluoride can lead to fluorosis of teeth and bones (Gbadebo, 2012). Chronic intake of fluoride may also lead to muscle fiber degeneration, low hemoglobin level, excessive thirst, skin rashes, depression, growth retardation, and DNA structural changes (Gbadebo, 2012; Meenakshi and Maheshwari, 2006). Fluoride is mainly released into groundwater via slow dissolution of geogenic fluoride bearing minerals such as fluorite, fluorospar, cryolite, theorapatite, phosphorite, apatite, topaz, villiaumite, sepiolite, and palygorskite in rocks (Banerjee, 2015; Jagtap et al., 2012; Yadav et al., 2018). Fluoride is also generated by industries producing glass and ceramics, chemicals and metals with effluent from these industries having fluoride levels ranging from 10 to 10,000 mg/L (Bhatnagar et al., 2011). The world health organization (WHO) recommends a threshold of 1.5 mg F<sup>-</sup>/L in drinking water (WHO, 2004). The United States Environmental Protection Agency (USEPA) has established a maximum contaminant level (MCL) of 4 mg/L to prevent skeletal fluorosis and a secondary maximum contaminant level (SMCL) of 2 mg/L to protect against dental fluorosis in human (USEPA, 2009). More than 260 million people worldwide use drinking water containing fluoride in excess of the WHO recommended limit of 1.5 mg/L (Amini et al., 2008; Jagtap et al., 2012).

While precipitation/coagulation, membrane processes, ion exchange, and adsorption are used for fluoride removal from drinking water (Meenakshi and Maheshwari, 2006; Mohapatra et al., 2009), adsorption is the most widely used because of its low cost, simple design, high removal efficiency, and economic viability (Bhatnagar et al., 2011). Activated carbon (Araga and Sharma, 2017; Araga et al., 2017; Chen et al., 2017; Rashid and Bezbaruah, 2020), carbon-based composites (Di et al., 2007; Kuang et al., 2017; Ruan et al., 2017; J. Zhang et al., 2019), metal oxides (Mukhopadhyay et al., 2017), alum sludge (Sujana et al., 1998), metal-organic frameworks (MOFs) (Karmakar et al., 2016), nanoscale zero-valent iron (Cao et al., 2021) and layered double hydroxides (Lv et al., 2007) are the popular adsorbents for fluoride removal. Among them, rare earth metal oxides have shown high binding affinities for fluoride (Chigondo et al., 2018b; Li et al., 2010; Mukhopadhyay et al., 2017; Y.Y. Zhang et al., 2019). The mechanism of fluoride removal by metal oxides involves the exchange between fluoride ions and surface hydroxyl groups of the adsorbents (Karmakar et al., 2016; Yu et al., 2018). The hydroxyl groups either exist on the metal hydroxide surface or can be formed through the hydroxylation of metal oxides and metal organic frameworks in aqueous environments (Wendt et al., 2006).

Among the rare earth metal oxides, cerium oxide (Ceria,  $CeO_2$ ) has been used for aqueous arsenic (Sakthivel et al., 2017), chromium (Xiao et al., 2009), lead (Sharma et al., 2018), mercury (Sharma et al., 2018), and organic dyes (Yu et al., 2015) removal. Ceria exhibits facile transformation between +3 and +4 oxidation states depending on

the redox environment making it a versatile adsorbent for various contaminants (Chigondo et al., 2018b; McCormack et al., 2014; Sakthivel et al., 2017). Cerium-loaded mesoporous zirconium phosphate (Dash et al., 2015), carbon nanotube supported ceria nanoparticles (Di et al., 2007), cubical ceria nanoparticles (Dhillon et al., 2016), CeO<sub>2</sub>-ZrO<sub>2</sub> nanocages (Wang et al., 2013), hydrous cerium-magnesium oxides (Chigondo et al., 2018b), and cerium(IV)-incorporated hydrous iron (III) oxide (Mukhopadhyay et al., 2017) have been reported to remove fluoride. However, these ceria-based materials needed 40-2750 min contact time to remove fluoride (Table 1) (Chigondo et al., 2018b; Dash et al., 2015; Dhillon et al., 2016; Di et al., 2007; Mukhopadhyay et al., 2017; Wang et al., 2013; J. Zhang et al., 2019), and that limits their use as a high contact time translates to a large reactor (filter) volume. Other materials with high fluoride adsorption capacity such as MOFs (Karmakar et al., 2016), layered double oxides (Lv et al., 2007), and composites of different metal oxides (Liu et al., 2016) have also shown slow adsorption kinetics.

Additionally, typical ceria nanoparticles are 3–12 nm in size (Zhang et al., 2002) and they agglomerate quickly (Rohder et al., 2014; Safi et al., 2010) and that limits their use in the aqueous environment. The agglomeration problem can be addressed by embedding (decorating) ceria nanoparticles onto graphene oxide sheets (Sakthivel et al., 2017). Graphene oxide (GO) provides a unique two-dimensional (2-D) platform with high specific surface area (theoretical value = ~2400 m²/g (Zhang et al., 2020)), low bulk density  $(0.06-0.3~g/cm^3)$  (Kovtun et al., 2019)), high oxygen-containing functional group density (C/C) ratio: 2–4 (Perreault et al., 2015)), and unique physicochemical properties (Mkhoyan et al., 2009; Perreault et al., 2015). Further, its two available basal planes can support nanomaterials (Perreault et al., 2015).

This paper reports for the first time the use of a GO-CeO<sub>2</sub> nanohybrid (ceria nanoparticles supported on GO sheets, referred to as GO-CeO<sub>2</sub> in this paper) to remove aqueous fluoride. We hypothesized that the GO support will keep the ceria nanoparticles (CeO<sub>2</sub> NPs) as discrete entities (non or less agglomerated) and help in aqueous dispersion. Further, the GO sheets will also act as electron mediators and help in maintaining enough Ce<sup>3+</sup> in the nanohybrid for effective adsorption of fluoride. Specifically, the role of the GO sheets as electron reservoirs and how that helps in fluoride removal have been explored. The fluoride adsorption capacity of GO-CeO<sub>2</sub> (nanohybrid) was tested under various experimental conditions of pH, the presence of co-existing anions, and ionic strength. A possible fluoride removal mechanism has been proposed based on experimental results and characterization data.

#### 2. Materials and methods

# 2.1. Materials

All chemicals were used as received unless otherwise specified. A multi-layered graphene oxide (GO) was obtained from Garmor, Inc.

**Table 1**Comparison of fluoride removal by different ceria-based material.

Adsorbent	рН	Dosing (g/L)	Initial conc (mg/L)	Contact time (min)	Sorbent/sorbate (g/mg)	% removal	Source
Hydrous CeO <sub>2</sub> -Fe <sub>3</sub> O <sub>4</sub> decorated polyaniline fibers	6.0	0.6	40	120	0.015	90.0	(Chigondo et al., 2018b)
CeO <sub>2</sub> -Rod	3.5	0.5	50	2750	0.010	70.0	(Kang et al., 2017)
Mn-Ce oxide	6.0	0.1	10	180	0.010	73.5	(Deng et al., 2011)
Ce-Fe bimetal oxides	NR	0.5	10	40	0.050	90.0	(Tang and Zhang, 2016)
CeO <sub>2</sub> -ZrO <sub>2</sub> nanocages	4.0	0.2	10	1440	0.020	70.0	(Wang et al., 2013)
Cerium (IV)-incorporated hydrous iron(III) oxide	7.0	0.5	10	120	0.050	85.0	(Mukhopadhyay et al., 2017)
Cerium loaded mesoporous zirconium phosphate	6.0	1.0	10	60	0.100	84.7	(Dash et al., 2015)
Cubical ceria nanosorbent	7.0	1.0	10	120	0.100	95.0	(Dhillon et al., 2016)
Mg-Al-Ce triple-metal composites	7.0	0.2	50	180	0.004	38.0	(Chi et al., 2017)
GO-CeO <sub>2</sub> nanohybrid	6.5	1.0	10	1	0.100	85.0	This work
	4.0					100.0	

(Orlando, FL) and used without further modification. The list of chemicals is in SI (Section S1.1).

#### 2.2. Synthesis of GO-CeO2 nanohybrid

The GO-CeO<sub>2</sub> was synthesized in a one-pot hydrothermal synthesis process using GO and cerium(III) nitrate hexahydrate as the starting materials as per our previously published method (Sakthivel et al., 2017). Details in SI (Section S1.2).

#### 2.3. Characterization

High-resolution transmission electron microscopy (HRTEM), Scanning Electron Microscopy (SEM), X-ray photoelectron spectroscopy (XPS), and a Zetasizer were used for material characterization. Details in SI (Section S1.3).

#### 2.4. Batch studies

The batch kinetic, isotherm and interference studies were conducted with GO-CeO $_2$  and control experiments were run with GO or CeO $_2$  nanoparticles as needed. The kinetic studies were conducted at an initial fluoride concentration ( $C_0$ ) of 10 mg/L over time. Isotherm studies were carried out by varying the  $C_0$  from 5 to 40 mg/L. The effect of pH was evaluated in the pH range of 4 to 10. The interference study was conducted using different concentrations of sulfate ( $SO_4^{-}$ ), phosphate ( $PO_4^{3}$ -P), bicarbonate ( $PCO_3^{-}$ ), chloride ( $PCO_3^{-}$ ), and nitrate ( $PCO_3^{-}$ -N). In this study we used SPADNS method (UV spectrophotometer) to detect fluoride in water (Hach, Model DR 5000, Method 8029, detection range: 0.02–2.00 mg/L). Details in SI (Section S1.4 and S1.5)

#### 2.5. Quality control and statistical analysis

All experiments were conducted in triplicates and the average values are reported here along with the standard deviations. One-way ANOVA analysis was done using Minitab to determine statistically significant differences in the data sets and Tukey's pairwise comparison was used to identify the data that were significantly different.

#### 3. Results and discussion

#### 3.1. Characterization

The nanostructure and morphology of the GO-CeO<sub>2</sub> were observed in TEM micrographs (Fig. 1a–b). The CeO<sub>2</sub> NPs (some dispersed and some aggregated, Fig. 1b) were attached onto the GO sheet (gray sheet, Fig. 1a) and the CeO<sub>2</sub> NPs were 10–20 nm in the size (Fig. 1b). HRTEM image (Fig. 1c) shows the crystallites with an estimated d-spacing 0.327 nm relating them to (111) plane of CeO<sub>2</sub> (cubic

structure). These findings are in agreement with previous report (Sakthivel et al., 2017). The morphology of  $GO-CeO_2$  was also studied using SEM. SEM micrographs show that  $GO-CeO_2$  has a flaky structure with irregular size and shape (Fig. 1d).

Zeta potentials ( $\zeta$ ) of GO, CeO<sub>2</sub> NPs, and GO-CeO<sub>2</sub> were measured in 0.01 M NaCl medium (solution pH ~7). The GO remained well dispersed in aqueous media due to its high  $\zeta$  ( $-42.99 \pm 1.73$  mV). Particles with  $\zeta$  >  $|\pm 25|$  mV are known to make a stable suspension (ISO, 2000). While CeO<sub>2</sub> NPs with their low  $\zeta$  (3.18  $\pm$  0.28 mV) agglomerated easily, the GO-CeO<sub>2</sub> with a high  $\zeta$  (33.99  $\pm$  0.44 mV) made a stable dispersion.

#### 3.2. Batch studies

#### 3.2.1. Effectiveness of GO-CeO2

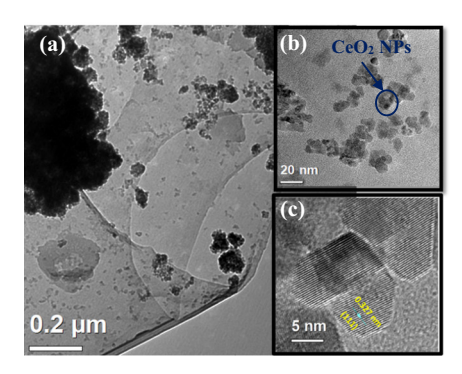
The comparison of fluoride removal efficiency of GO-CeO<sub>2</sub> and the controls (CeO<sub>2</sub> NPs and GO) showed that the GO-CeO<sub>2</sub> has a high removal efficiency (85%) which is significantly higher than that of CeO<sub>2</sub> NPs (12% fluoride removal,  $p=0.000,\,\alpha=0.05)$  or GO (1%,  $p=0.000,\,\alpha=0.05)$  used alone (Fig. 2a). The potential quick aggregation of CeO<sub>2</sub> NPs (when used alone) might have decreased their reactivity (Safi et al., 2010) and they exhibited poor fluoride removal efficiency (12%). However, the nanohybrid had an improved fluoride removal efficiency which was ~73% higher compared to only CeO<sub>2</sub> NPs. It is logical to infer that the use of GO as a platform for CeO<sub>2</sub> NPs increased the reactivity of the nanoparticles and enhanced fluoride removal was achieved. Enhanced dispersion ( $\zeta$  of 33.99  $\pm$  0.44 mV) of the nanohybrid potentially influenced fluoride removal (also see Fluoride Removal Mechanisms).

# 3.2.2. Effect of adsorbent dose

At  $C_0 = 10$  mg F $^-$ /L, fluoride removal efficiency increased from 18% to 100% with the increase of adsorbent (GO-CeO $_2$ ) dosage from 0.2 to 1.5 g/L (Fig. 2b). Given, the recommended WHO threshold of 1.5 mg F $^-$ /L in drinking water, the optimal adsorbent dose was decided as 1 g/L (85% removal) in this study; this dosing was sufficient to achieve the recommended WHO limit for fluoride in drinking water and keeping some fluoride in the water for human nutritional requirements. Similar adsorbent doses were reported by others (Table 1). All experiments reported henceforth used 1 g/L of the nanohybrid.

# 3.2.3. Kinetics

The results of fluoride removal by GO-CeO $_2$  over time (till 120 min,  $C_0=10~mg~F^-/L$  and adsorbent dose of 1 g/L) showed that the fluoride adsorption by GO-CeO $_2$  follows very fast kinetics (Fig. 2c) compared to the materials reported by others including MOFs, mesoporous ZrO $_2$ , GO-Zr, and Ce-Zr composites (Chen et al., 2016a; Karmakar et al., 2016; Mohan et al., 2016; Wang et al., 2017; Yu et al., 2018; Zhang et al., 2017). GO-CeO $_2$  achieved 85% fluoride adsorption within 1 min and reached equilibrium at the same time (Fig. 2c inset). We have



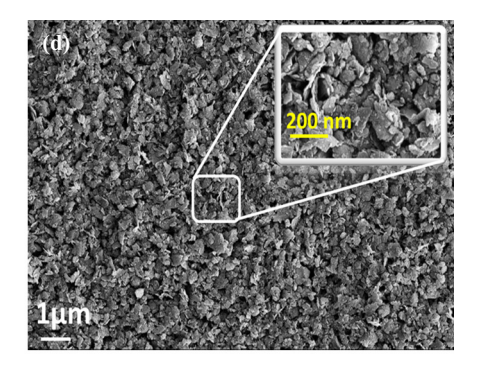


Fig. 1. (a) TEM micrograph of the GO-CeO<sub>2</sub> (nanohybrid) at lower magnification. The micrograph shows that the ceria particles (black dots) are present on the graphene oxide matrix (gray sheet); (b) TEM micrograph at higher magnification show the CeO<sub>2</sub> NPs deposited on the GO sheets were 10–20 nm in size; (c) HRTEM image of the GO-CeO<sub>2</sub> shows the crystallites with an estimated d-spacing 0.327 nm relating them to (111) plane of CeO<sub>2</sub> (cubic structure); and (d) SEM micrographs of GO-CeO<sub>2</sub> show that it has a flaky structure.

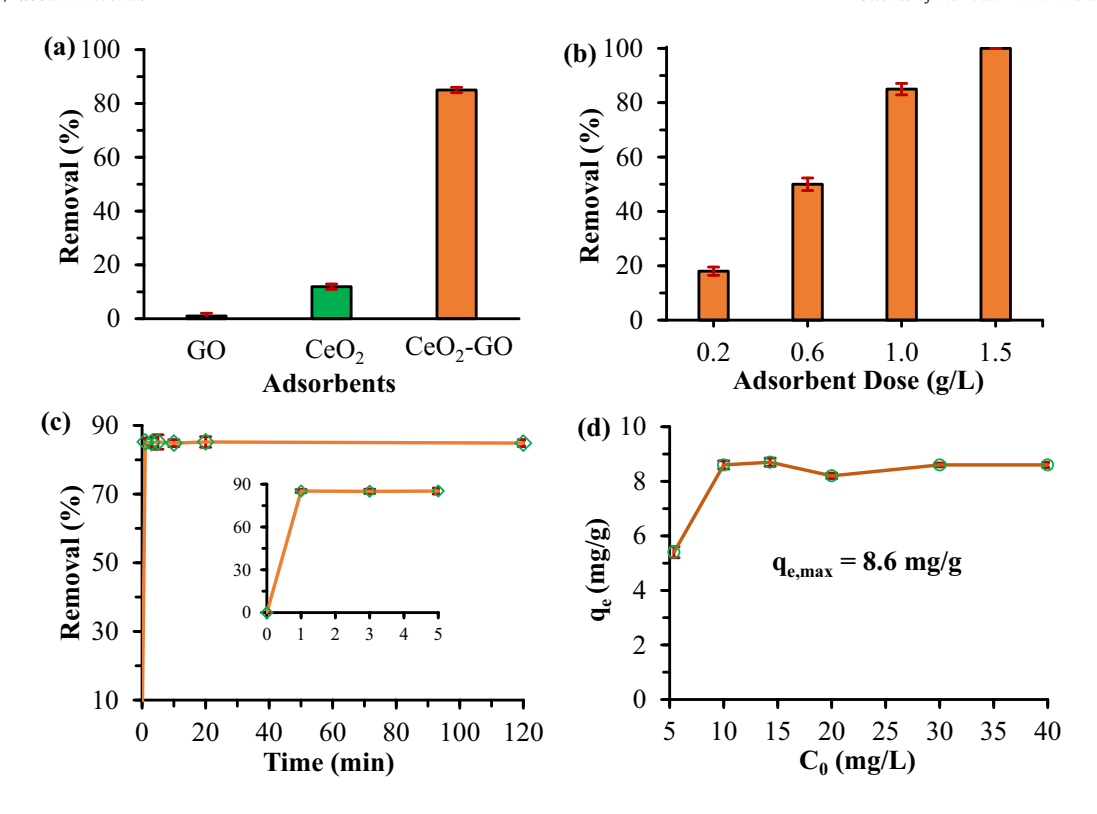


Fig. 2. (a) Fluoride removal by GO-CeO<sub>2</sub> and the controls (CeO<sub>2</sub> NPs and GO); adsorbent dose = 1 g/L;  $C_0 = 10$  mg  $F^-/L$ ; (b) Effect of GO-CeO<sub>2</sub> dosing on fluoride removal. Dosing of 1 g/L yielded 85% fluoride removal ( $C_0 = 10$  mg  $F^-/L$ ) reducing bulk fluoride concentration to 1.5 mg  $F^-/L$  (WHO recommended limit for drinking water), and so 1 g/L was selected as the optimal dose; (c) Removal of fluoride by GO-CeO<sub>2</sub> over time ( $C_0 = 10$  mg  $F^-/L$ ) (Inset: Initial 5 min data zoomed in). The fluoride removal reached equilibrium within 1 min which is one of the fastest fluoride removal kinetics reported so far; and (d) Fluoride adsorption capacity of GO-CeO<sub>2</sub> at different concentrations of fluoride. The maximum fluoride adsorption capacity was found to be 8.6 mg/g. GO-CeO<sub>2</sub> dose = 1 g/L and initial pH 6.5. The data points are connected with straight lines for ease of reading only and they do not represent trendlines, and the vertical error bars represent  $\pm$  standard deviations.

compared the results with other reported ceria-based materials (Table 1) and as well as other standard materials (activated carbon, activated alumina, and calcium-based adsorbents) (Table S1). Our material showed ultra-rapid kinetics which is 40-2750 times faster than other ceria-based materials (nano and non-nano, Table 1) and 20-780 times faster than the typical (non-nano, Table S1) fluoride adsorbents even when high adsorbent doses were used by others. For example, Ce-Fe bimetal oxides reached equilibrium (90% fluoride removal) in 40 min and our nanohybrid needed 1 min to reach equilibrium (85% fluoride removal). Therefore, our nanohybrid exhibited kinetics which is 40 times faster than the Ce-Fe bimetal oxides, Again, contact time to reach equilibrium in fluoride removal (70%) by CeO<sub>2</sub>-Rod was 2750 min, and that makes our nonhybrid kinetically 2750 times faster than CeO<sub>2</sub>-Rod. This makes GO-CeO<sub>2</sub> much superior to all previously reported fluoride adsorbents. To rule out the dose-effect (sorbent to sorbate ratio) on the observed fast kinetics, additional kinetic studies were conducted with different GO-CeO<sub>2</sub> dosages (0.2 to 1.0 g/L). The rapid kinetics (equilibrium reached in 1 min) was observed irrespective of the sorbent to sorbate ratio used (SI, Fig. S1) indicating that the rapid kinetics was not affected by the sorbent dose used and, hence, other factors might have played roles. This rapid adsorption translates to a short detention time which will lead to a small reactor (treatment unit) volume and thus reduced infrastructure cost. With its fast reaction kinetics, GO-CeO2 is a potential candidate for use in high throughput defluoridation systems for both point-of-use and centralized water treatment systems.

The kinetic study data were fitted into the Webber-Morris intraparticle diffusion model (Weber and Morris, 1963) (Eq. (1)) to find out the potential rate-controlling steps such as film diffusion or intraparticle diffusion.

$$\boldsymbol{q}_t = \boldsymbol{K}_p t^{0.5} \tag{1}$$

In Eq. (1),  $K_p$  is the intra-particle diffusion rate in  $mg/g/min^{0.5}$  and  $q_t$ is the adsorption capacity (mg/g) at time t. If the plot of  $q_t$  vs  $t^{0.5}$  passes through the origin then intra-particle diffusion is the only ratedetermining step. In this study, the plot showed bilinearity (SI, Fig. S2) with the first section (solid line) representing the external mass transport across the boundary layer, and the second section (dashed line) being the equilibrium stage (Sadeghi et al., 2020). The equilibrium was reached within 1 min, we could not get any data points between 0 min and 1 min to investigate intra-particle diffusion which might have occurred during that time along with film diffusion. Sadeghi et al., while treating arsenic with graphene oxide nanoribbons achieved near-equilibrium within 2 min and reported that both intra-particle diffusion and film diffusion participated in the removal process (Sadeghi et al., 2020). While we cannot conclusively prove that intra-particle diffusion took place, it is highly likely given the structure of our nanohybrid. In the multi-layered GO we used, CeO<sub>2</sub> NPs were decorated on both faces of each GO sheet and a stacked GO-CeO2 was formed. Others also reported similar nanoparticle deposition patterns (Wu et al., 2012). Fluoride ions might have interacted with the CeO<sub>2</sub> nanoparticles inside the staked layers via intra-particle diffusion. We can infer that both intra-particle diffusion and film diffusion were ratelimiting in our experiment with the caveat that we did not have any experimental data points between 0 and 1 min.

#### 3.2.4. Isotherm studies

The maximum fluoride adsorption capacity ( $q_{e,max}$ ) of GO-CeO $_2$  was found to be 8.60 mg/g (initial pH 6.5) (Fig. 2d). We also conducted isotherm studies at pH 4 (SI, Fig. S3) as maximum fluoride removal was achieved at pH 4 (see Effect of pH) and the maximum adsorption capacity increased to 16.07 mg/g. However, 8.60 mg/g at near-neutral pH is the more relevant value. We compared our result with two conventional adsorbents (acidic alumina and granular activated alumina)

(Ghorai and Pant, 2005; Goswami and Purkait, 2012) typically used for drinking water fluoride removal. Our nanohybrid recorded similar adsorption capacity as the acidic alumina (AA, adsorption capacity 8.4 mg/g) and acted 3.5 times better than the granular activated alumina (GAA, 2.41 mg/g). While GAA was tested at pH 7, AA was effective at pH 4.4 only. Dissolution of aluminum complexes from aluminum-based adsorbent poses a human health risk as aluminum ion and its aluminofluoride complexes are known neurotoxins (Martyn et al., 1989; Strunecka and Patocka, 1999), so use of AA and GAA are increasingly being questioned (George et al., 2010). Further, our nanohybrid exhibited kinetics which is 90 times faster compared to AA and 360 times faster than GAA, and that too at near-neutral pH (6.5), making it a superior adsorbent for use in a high throughput defluoridation system.

To determine the relationship between adsorbent and adsorbate, and to understand the mechanism(s) of fluoride removal, the experimental adsorption data were fitted onto Freundlich and Langmuir isotherm models (SI, Section S2.4). The data fitted well onto Langmuir isotherm (R² = 0.9995) rather than Freundlich (R² = 0.0103) (SI, Fig. S4) indicating that the adsorption of fluoride by GO-CeO₂ is a monolayer and homogenous phenomenon, and the maximum adsorption capacity calculated as 8.61 mg/g (Table 2) which tallies with our experimental value (8.60 mg/g). The dimensionless constant  $R_L$  values calculated for the fluoride concentrations (5, 10, 20, 30, and 40 mg/L) used in this study are in the range of 0.003–0.025 (between 0 and 1) (Table 2) suggesting that fluoride adsorption onto GO-CeO₂ is favorable.

# 3.2.5. Effect of pH

As the pH increased from 4 to 6 a significant decrease (100% to 83%,  $p = 0.000, \alpha = 0.05$ ) in fluoride removal was observed and the removal efficiency gradually decreased to 66% at pH 10. The point-of-zerocharge (PZC) of GO-CeO<sub>2</sub> was measured as 2.7 (Fig. 3b). The surface of the nanohybrid remained positively charged below pH 2.7, and took up the fluoride ions electrostatically (Dash et al., 2015; Dhillon et al., 2016; Mukhopadhyay et al., 2017; Wang et al., 2013). The maximum fluoride removal was achieved at pH 4. At pH » PZC, the F<sup>-</sup> removal efficiency decreased significantly (Fig. 3a) due to the generation of negative charges on the adsorbent surface engendering repulsion for the fluoride ions. Further, at higher pH, more OH<sup>-</sup> were available near the GO-CeO<sub>2</sub> surface competing for available adsorption/ionexchange sites (Chai et al., 2013; Dash et al., 2015). However, the efficiency of fluoride removal did not go down below 66% even at pH 10 indicating that the fluoride removal by GO-CeO<sub>2</sub> was not dominated by electrostatic interaction only but chemisorption was also possibly involved.

# 3.2.6. Effect of co-existing ions

Groundwater contains anions such as chloride (Cl $^-$ ), nitrate (NO $_3^-$ ), bicarbonate (HCO $_3^-$ ), sulfate (SO $_4^-$ ), and phosphate (PO $_3^+$ ) in addition to fluoride in contaminated waters. The potential interferences by coexisting ions were examined by adding individual interfering anions (Cl $^-$ , NO $_3^-$ , PO $_3^+$ , HCO $_3^-$ , and SO $_4^+$ ; 0, 10, and 100 mg/L) to the bulk fluoride solution (C $_0^-$  = 10 mg/L and adsorbent dose = 1 g/L). The concentration range was selected based on actual chemical composition of groundwater contaminated with fluoride (Narsimha and Sudarshan, 2017; Bhagawan et al., 2019; Thakur and Mondar, 2017). In case of phosphate, 100 mg/L is not a relevant concentration. However, to

**Table 2**Adsorption isotherm parameters for fluoride adsorption onto GO-CeO<sub>2</sub> nanohybrid.

Langmuir iso	therm	Freundlich isotherm <sup>a</sup>		
q <sub>m</sub> (mg/g)	b (L/mg)	$R^2$	$R_L$	$R^2$
8.61	7.9	0.9995	0.003-0.025	0.0103

<sup>&</sup>lt;sup>a</sup> The isotherm parameters for Freundlich isotherm are not shown as the R<sup>2</sup> value is very low meaning the data do not fit the model.

keep the concentration range same for all interfering ions 100 mg/L was used for phosphate as well. Significant interferences (p =0.000-0.037,  $\alpha = 0.05$ ) in fluoride adsorption was observed in the presence of all anions (Fig. 3c). However, Cl<sup>-</sup> and NO<sub>3</sub> showed the least effect (85% fluoride removal with no Cl<sup>-</sup> and NO<sub>3</sub> -N, 83% at 100 mg Cl<sup>-</sup>/L and 80% at 100 mg NO<sub>3</sub>-N/L); Cl<sup>-</sup> and NO<sub>3</sub> being a low-affinity ligand did not compete for the fluoride adsorption sites (Chen et al., 2016b; Mohanty et al., 2005). The presence of PO<sub>4</sub><sup>3-</sup> significantly decreased fluoride removal from 85% (no  $PO_4^{3-}$ -P) to 46% (10 mg  $PO_4^{3-}$ -P/L) and then to  $\sim 7\%$  (100 mg PO<sub>4</sub><sup>3</sup>-P/L). The presence of SO<sub>4</sub><sup>2</sup> also significantly decreased fluoride removal from 85% (no  $SO_4^{2-}$ ) to 56% (10 mg  $SO_4^{2-}/L$ ) and then to  $\sim 38\%$  (100 mg  $SO_4^{2-}/L$ ).  $HCO_3^{-}$  also showed a significant negative effect on fluoride removal (dropped to 19% at 100 mg/L) possibly because of hydrolysis of  $HCO_3^-$  ( $HCO_3^- + H_2O \Rightarrow H_2CO_3 + OH^-$ ) leading to more OH<sup>-</sup> being present to compete with fluoride for the adsorption sites (Deng et al., 2011; Wang et al., 2013). The order of interference of the co-existing anions was  $PO_4^{3-} > HCO_3^{-} > SO_4^{2-} > NO_3^{-} > Cl^{-}$ . The order of interference is related to the charge/radius (Z/R) values of the competing anions (except  $HCO_3^-$ ):  $PO_4^{3-}$  (3/3.40) >  $SO_4^{2-}$  (2/2.40) >  $NO_3^-$  (1/2.81) > Cl<sup>-</sup> (1/1.81). The greater the Z/R, the more likely that the specific anion was attracted to the adsorbent surface leading to more interference with fluoride adsorption (Liu et al., 2016; Zhao et al., 2010). Working with cubical ceria (Dhillon et al., 2016), ceria-iron bimetal oxides (Tang and Zhang, 2016), and CeO<sub>2</sub>-Fe<sub>3</sub>O<sub>4</sub> decorated polyaniline fibers nanocomposite (Chigondo et al., 2018a), others have observed interferences from PO<sub>4</sub><sup>3-</sup> (Chigondo et al., 2018a), HCO<sub>3</sub><sup>3</sup> (Tang and Zhang, 2016),  $SO_4^{2-}$  (Dhillon et al., 2016), and  $NO_3^{-}$ (Dhillon et al., 2016) (SI, Table S2). The typical concentration of phosphate in groundwater is <100 µg/L, and therefore, will have minimal effect on fluoride removal by GO-CeO<sub>2</sub>. The interference by bicarbonate can be minimized by adjusting the pH ( $\leq$ 7.0). Pretreatments may be necessary to reduce the interferences of some of the ions. Narsimha and Sudarshan (2017) reported that SO<sub>4</sub><sup>2-</sup> concentration in groundwater in one of the worst fluoride affected areas in India varied from 21 to 137 mg/L; we expect GO-CeO<sub>2</sub> to work reasonably well with low sulfate concentration but more adsorbent may be needed to treat water with high sulfate levels.

# 3.2.7. Effect of ionic strength

The effect of ionic strength on fluoride adsorption by GO-CeO<sub>2</sub> was evaluated ( $C_0 = 10 \,\mathrm{mg}\,\mathrm{F}^-/\mathrm{L}$ ) to find out whether the outer-sphere complexation (electrostatic interaction) was participating in fluoride removal. The fluoride removal efficiency decreased from 85% to 59% with the increase of ionic strength from 0 M to 1 M (Fig. 3d) indicating that the electrostatic interaction significantly impacted the overall fluoride adsorption onto GO-CeO<sub>2</sub>. The outer-sphere complexes were suppressed when ionic strength increased due to the competition between the electrolyte ions (i.e., Cl<sup>-</sup>) and adsorbing anions (F<sup>-</sup> here) for available surface sites (Liu et al., 2015). The electrolyte concentration might have also affected the interfacial potentials and that led to a decrease in adsorption activity as suggested by Hayes et al. (1988). The electrolyte ions and outer-sphere complexes are present in the same plane ( $\beta$ -plane of the diffuse double layer around the adsorbent surface) in a bulk solution (Hayes et al., 1988). Therefore, outer-sphere complexes are expected to be more sensitive than the inner-sphere complexes to ionic strength variation. We can infer that outer-sphere complexation (electrostatic interaction) was contributing to fluoride removal in this study.

# 3.2.8. Desorption study

A desorption study was conducted over a 3-month period to find out the stability of fluoride adsorbed onto the  $GO-CeO_2$ . Batches of  $GO-CeO_2$  (20 mg) were saturated with fluoride by putting the nanohybrid in 20 mL of fluoride solution (10 mg/L) in 40 mL glass vials and shaking the vials end-over-end for 24 h. The saturated  $GO-CeO_2$  were then separated and the bulk solution fluoride concentration was measured to

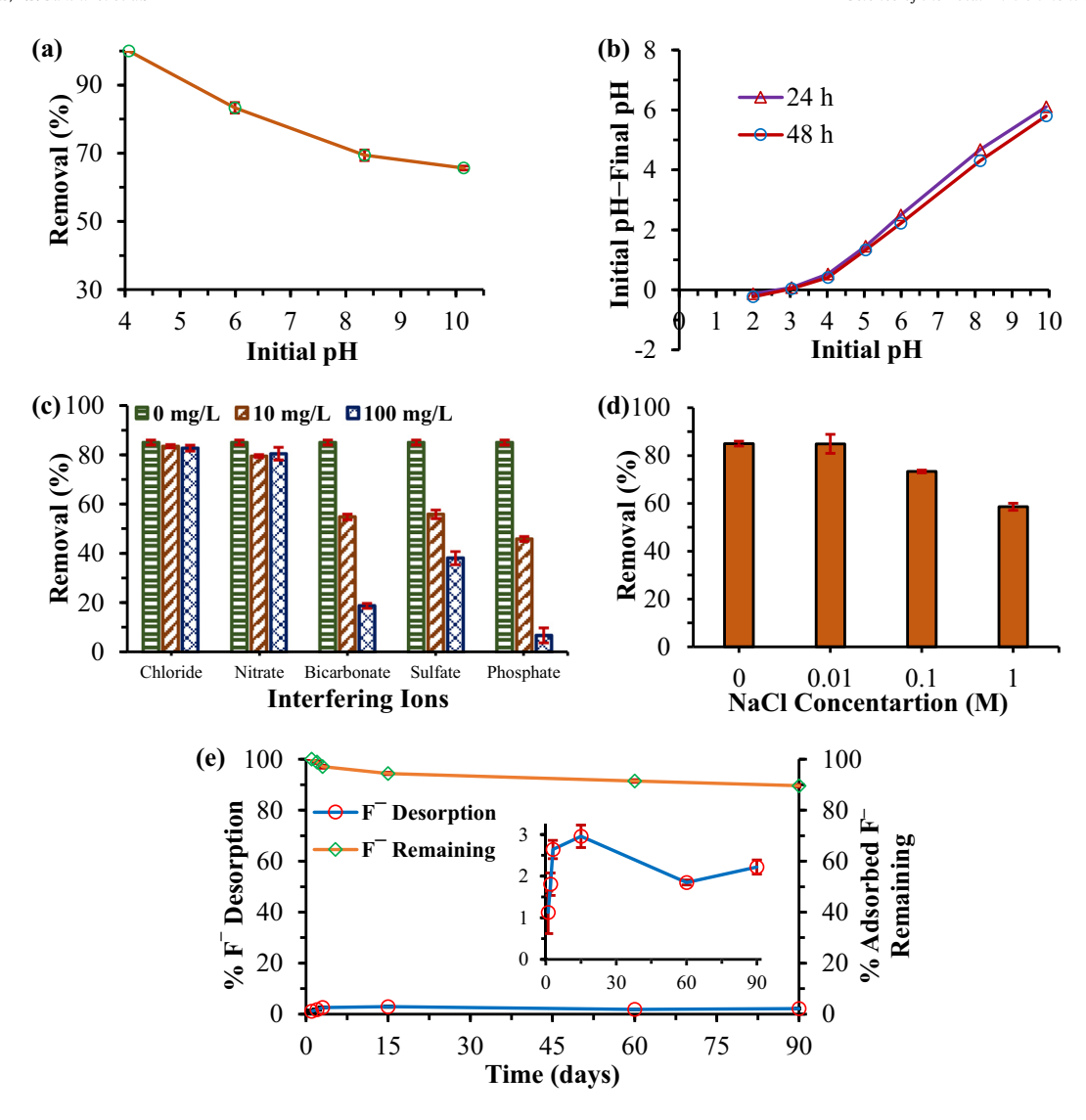


Fig. 3. (a) Effect of initial pH on fluoride adsorption onto GO-CeO<sub>2</sub>; (b) Point-of-Zero-Charge (PZC) of GO-CeO<sub>2</sub> was found to be 2.7; (c) Effect of co-existing ions on fluoride adsorption onto GO-CeO<sub>2</sub>. The order of interference is  $PO_4^2 > PO_3 > SO_4^2 > NO_3 > CI^-$ . The concentration of nitrate is in mg  $PO_3^2 - NL$  and phosphate concentration is in mg  $PO_3^2 - P/L$ ; and (d) Effect of ionic strength on fluoride removal by GO-CeO<sub>2</sub>. While there was no significant change at 0.01 M NaCl (compared to 0 M NaCl), the fluoride removal efficiency decreased with the increase of ionic strength beyond 0.01 M. The findings indicated that the outer-sphere complexation also contributed to fluoride removal by GO-CeO<sub>2</sub>; and (e) Desorption of fluoride from the used GO-CeO<sub>2</sub> (Inset: percent desorption in 90 days with the Y-axis limited to 3.25%). The secondary axis shows fluoride adsorbed onto GO-CeO<sub>2</sub>. Note: The data points are connected with straight lines for ease of reading only and they do not represent trendlines, and the vertical error bars represent  $\pm$  standard deviations.

determine the amount of fluoride adsorbed by GO-CeO2. The decanted solution was then replaced with DI water and the contents (fluoride saturated GO-CeO<sub>2</sub> and DI water) were shook for another 24 h. After that, the GO-CeO<sub>2</sub> was separated again from the solution by centrifugation and the bulk solution was analyzed to estimate the amount of desorbed fluoride in the elapsed time. This process was continued at regular intervals for 3 months, and each time fresh DI water was used to replace the bulk solution. Results showed that the adsorbed fluoride remained strongly bound to GO-CeO<sub>2</sub> over the study period (Fig. 3e). About 1% of adsorbed fluoride got desorbed after the first day. After that only 1-2.8% of adsorbed fluoride got desorbed after each time period. After the 3-month time period, total fluoride desorbed was found to be 1.19 mg/g (11.9%). During fluoride removal by GO-CeO<sub>2</sub>, fluoride complexed with Ce<sup>3+</sup> to form insoluble coordination compound in the ceria lattice (Menon et al., 1986; Valicsek et al., 2019) (see Fluoride Removal Mechanisms), and for that reason desorption was not that high. The ~12% desorption observed in this study was possibly from the fluoride adsorbed onto GO-CeO<sub>2</sub> via outer-sphere complexation (electrostatic interaction).

# 3.3. Fluoride removal mechanisms

# 3.3.1. Mechanisms involved

In the pH studies (Fig. 3a), the maximum fluoride removal was recorded at pH 4 (>PZC, 2.7) and substantial removal occurred (~66%) even at pH 10. These observations indicate that not only electrostatic interaction was responsible for fluoride removal by GO-CeO<sub>2</sub> but chemisorption was also potentially playing a role.

The fluoride removal by  $\overline{\text{GO-CeO}_2}$  decreased with the increase of ionic strength (Fig. 3d) indicating outer-sphere complex formation and electrostatic interaction of fluoride with  $\overline{\text{GO-CeO}_2}$ . However, the presence of  $\overline{\text{PO}_4^{3-}}$  and  $\overline{\text{SO}_4^{2-}}$  significantly decreased fluoride adsorption onto  $\overline{\text{GO-CeO}_2}$  (Fig. 3c). Inner-sphere complexation governs the adsorption of  $\overline{\text{PO}_4^{3-}}$  (Dhillon et al., 2016; McCormack et al., 2014), and  $\overline{\text{SO}_4^{2-}}$  (Kuang et al., 2017) onto  $\overline{\text{CeO}_2}$ . Given that  $\overline{\text{PO}_4^{3-}}$  and  $\overline{\text{SO}_4^{2-}}$  interfered with fluoride adsorption in our study, it is safe to assume that  $\overline{\text{PO}_4^{3-}}$  and  $\overline{\text{SO}_4^{2-}}$  were targeting the same inner-sphere sites that fluoride would have otherwise occupied. So, we can infer that fluoride adsorption by  $\overline{\text{GO-CeO}_2}$  might have occurred due to the formation of inner-

sphere complexes as well. Others have reported similar phenomena where fluoride adsorption by ceria-based material was governed by inner-sphere complexation, and the presence of  $PO_4^{3-}$  and  $SO_4^{2-}$  significantly decreased the fluoride removal efficiency (Chigondo et al., 2018b; Dhillon et al., 2016; Kuang et al., 2017). While both outersphere and inner-sphere complexations played a significant role in fluoride removal by GO-CeO<sub>2</sub>, the substantial removal (~66%) at high pH (pH  $10 \gg PZC$ ) (Fig. 3a) and low desorption (~12%) from adsorbed phase during the desorption experiment (Fig. 3e) indicate that innersphere complexation (chemisorption) was more dominant than outer-sphere complexation.

To investigate the fluoride removal mechanism further, samples of the GO-CeO<sub>2</sub> before and after fluoride adsorption were characterized using XPS (Fig. 4). The peaks from the deconvoluted XPS Ce 3d spectra before and after fluoride adsorption (Fig. 4a) can be distinguished and ascribed to unique oxidation states. Peaks at ~880, 885, 898, and 903 eV belong to Ce<sup>3+</sup> oxidation state and peaks at ~882, 888, 899, 901, 908, and 917 eV belong to  $Ce^{4+}$  oxidation state (Seal et al., 2020). The XPS data have confirmed that the GO-CeO2 used in this study contained both Ce<sup>3+</sup> and Ce<sup>4+</sup> before and after fluoride adsorption. We synthesized GO-CeO<sub>2</sub> via a hydrothermal process at a high temperature (140 °C) in a closed reaction vessel. Exposure to high temperature and/or reducing gas conditions (i.e., low oxygen partial pressures) led to the loss of oxygen from ceria crystal surface to the gas phase, generating intrinsic oxygen vacancies (defects) (Dutta et al., 2006; Schmitt et al., 2020). In ceria lattice, when an oxygen vacancy is created, two electrons are released and those electrons reduce Ce<sup>4+</sup> to Ce<sup>3+</sup> oxidation state (Campbell and Peden, 2005; Schmitt et al., 2020; Sayle et al., 2016).

The concentration of  $Ce^{3+}$  before fluoride adsorption was 16% but increased to 34% after adsorption (Fig. 4a). The changes to the surface  $Ce^{3+}$  (or  $Ce^{4+}$ ) oxidation state after fluoride adsorption was also highly visible in the deconvoluted Ce 3d XPS spectrum. The increase of  $Ce^{3+}$  after fluoride adsorption indicates that additional oxygen vacancies were created in the ceria lattice (Ahmad et al., 2014). The chemical shifts and changes in valence state concentrations (Fig. 4a) of cerium on the surface of  $GO-CeO_2$  after fluoride adsorption reveal that charge transfer interaction occurred between the  $GO-CeO_2$  (adsorbent) and  $F^-$  ions. The C 1s spectral lines in the XPS spectra for the nanohybrid before and after fluoride adsorption (Fig. 4c) show that the peaks

belonging to GO (C—C/C=C, C—O—C, and O-C=O) have shifted (change in binding energies) after the adsorption of fluoride which also confirms the charge transfer interaction between  $GO-CeO_2$  and  $F^-$  ions.

In addition, the O 1s envelops were analyzed and deconvoluted into four peaks (C=0, C-0,  $Ce^{3+}$ - $O^{2-}$ , and  $Ce^{4+}$ - $O^{2-}$ , Fig. 4b) (Kang et al., 2017). The major peak at a binding energy of ~529 eV represents the lattice oxygen of  $Ce^{4+}-O^{2-}$  and the peak at a binding energy of ~530 eV can be ascribed to the Ce<sup>3+</sup>-O<sup>2-</sup> lattice oxygen (Ahmad et al., 2014; Kumar et al., 2009). Because the ionic radii of F<sup>-</sup> (0.133 nm) and  $O^{2-}$  (0.140 nm) are almost of the same size (Slater, 1964), the added fluoride in this study might have replaced the O<sup>2-</sup> ions in the ceria lattice via ion exchange (Fig. 5c, ii). This in turn led to a charge imbalance promoting conversion of Ce<sup>4+</sup> to Ce<sup>3+</sup> which is reflected in our XPS data (Ce<sup>3+</sup> concentration increased after adsorption, Fig. 4a). The reduced Ce3+ continuously adsorbed fluoride and made fluorine complex in the ceria lattice (Ahmad et al., 2014). The presence of a strong F 1s peak at binding energy ~684.5 eV (Fig. 5a) in our used (i.e., after fluoride adsorption) nanohybrid confirms the presence of the chemically bound fluoride in ceria lattice indicating that fluoride was effectively adsorbed by the GO-CeO<sub>2</sub>. A similar phenomenon was reported by Ahmad et al. (2014) where a fluoride-doped ceria nanocrystal was used for oxidative coupling of benzylamines, and they observed that the doped fluoride can occupy the oxygen sites of CeO<sub>2</sub> lattice and reported that Ce<sup>3+</sup> forms complex with F<sup>-</sup> ions. Further, they found a higher concentration of Ce<sup>3+</sup> upon fluoride doping because of charge compensation due to F<sup>-</sup> incorporation onto the O<sup>2-</sup> sites which is in line with our observation of reduction of  $Ce^{4+}$  to  $Ce^{3+}$ .

From the adsorption behavior and XPS data, we can propose that the removal of fluoride by  $GO\text{-}CeO_2$  happened in two steps (Fig. 5c): (1) first, fluoride was taken up by the nanohybrid electrostatically (outer-sphere complexation), and then (2) fluoride replaced  $O^{2-}$  and incorporated itself into the ceria lattice (inner-sphere complexation) releasing two electrons in the process. The released electrons reduced  $Ce^{4-}$  to  $Ce^{3+}$ , and the  $Ce^{3+}$  complexed with fluoride after adsorption.

### 3.3.2. Rapid kinetics and role of graphene oxide

To understand the rapid kinetics, we conducted a separate kinetic study with pristine CeO<sub>2</sub> NPs alone (not hybridized with GO), and

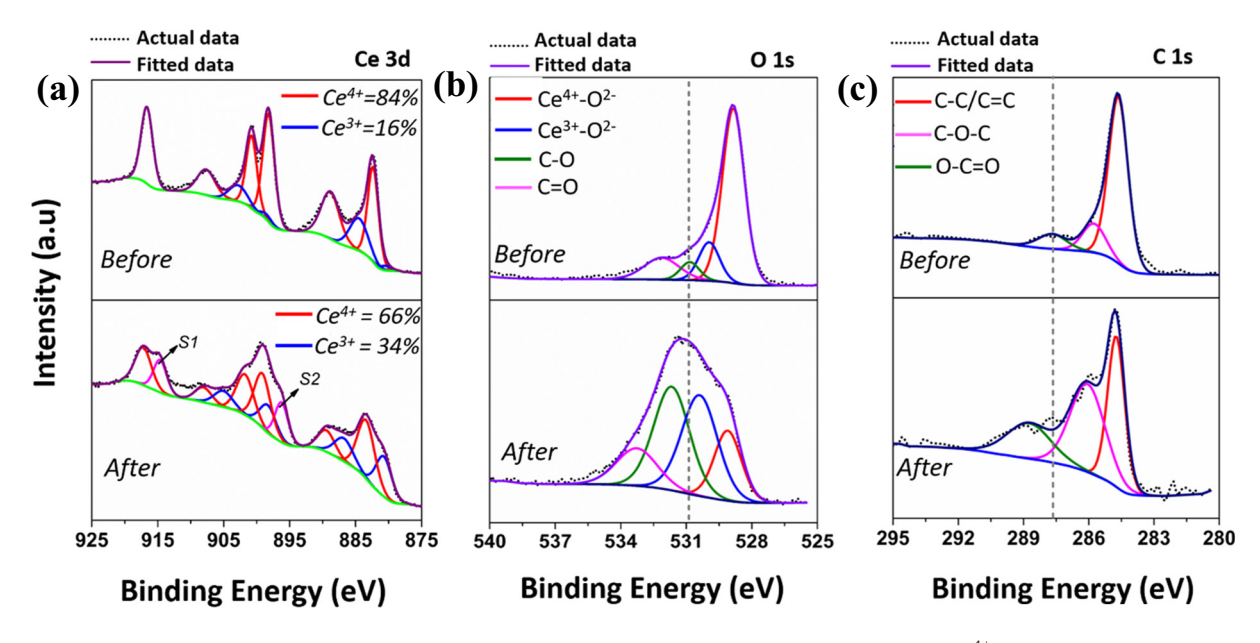


Fig. 4. XPS spectra of GO-CeO<sub>2</sub> (a) Ce 3d; (b) O 1s; and (c) C 1s before and after fluoride adsorption. The red line in Ce3d belongs to the Ce<sup>4+</sup> oxidation state and the blue line is for Ce<sup>3+</sup>. There are two additional peaks (S1 and S2) identified after fluoride adsorption, and they belong to the satellite peaks of Ce<sup>3+</sup>. The vertical dotted lines in O 1s and C 1s are for the ease of identification of the chemical shifts that occurred after fluoride adsorption.

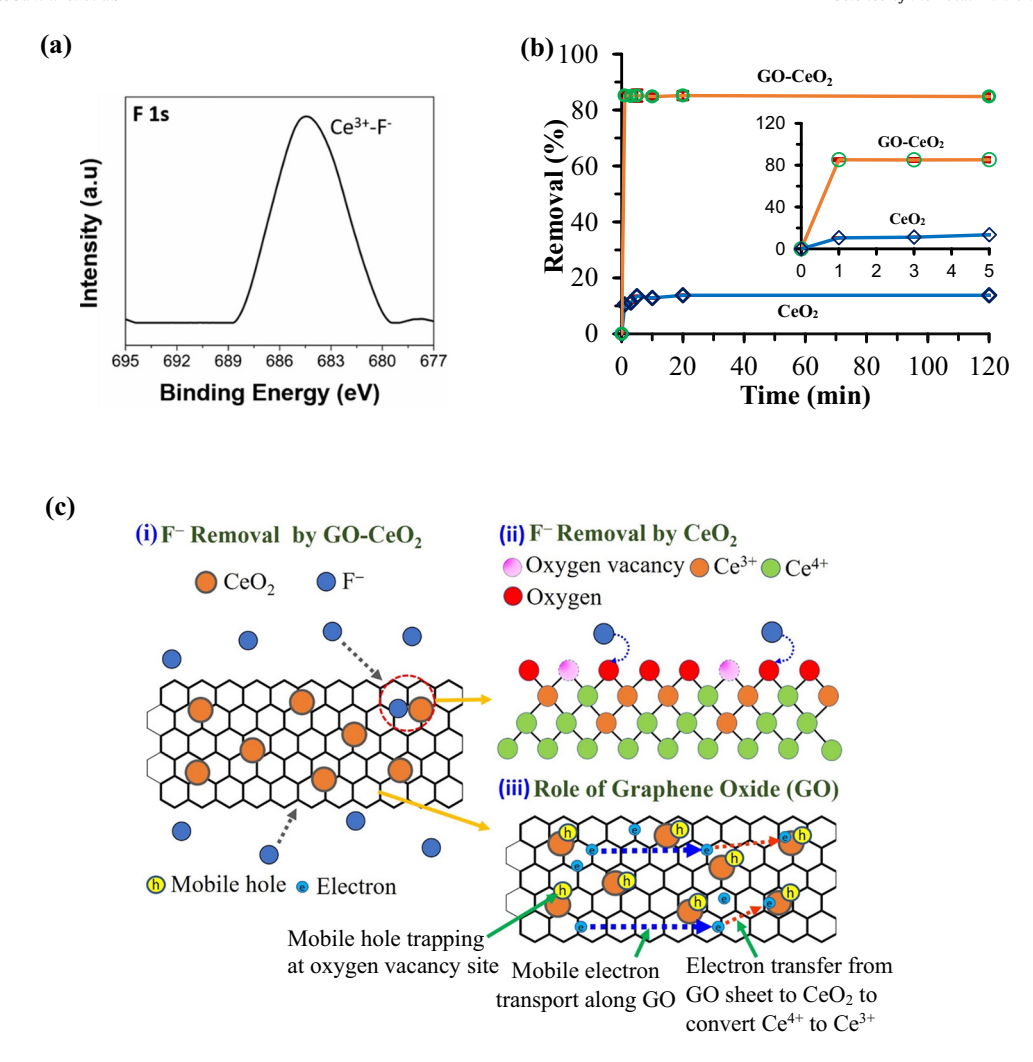


Fig. 5. (a) High-resolution XPS of F 1s spectrum after fluoride adsorption; (b) Fluoride removal by only  $CeO_2$  NPs; the plot for fluoride removal by GO- $CeO_2$  is also shown for ease of comparison (Inset: Initial 5 min data zoomed in). The data points are connected with straight lines for ease of reading only and they do not represent trendlines, and the vertical error bars represent  $\pm$  standard deviations; and (c) Schematic of the proposed mechanisms of fluoride removal by the GO- $CeO_2$  (i) the negatively charged fluoride ions move towards positively charged GO- $CeO_2$  and get adsorbed through electrostatic attraction; (ii) a ceria lattice with both  $Ce^{3+}$  and  $Ce^{4+}$  and surface oxygen vacancies, two ceria atoms coordinate with one oxygen atom. Fluoride replaces the surface  $O^{2-}$  by ion exchange process; and (iii) mobile holes of GO sheet are trapped by the oxygen vacancy sites in the ceria lattice which facilitate the mobile electron transport in the GO sheet. The mobile electrons can transfer to  $CeO_2$  at the  $CeO_2$  NP-GO interface and reduce  $Ce^{4+}$  to  $Ce^{3+}$ .

observed that even though  $CeO_2$  NPs exhibited poor removal of fluoride (13.4%), they exhibited fast kinetics till 1 min (Fig. 5b, SI, Fig. S5). It can be inferred that the rapid removal (adsorption/capture) of fluoride by  $GO\text{-}CeO_2$  was mostly because of the  $CeO_2$  NPs. When only  $CeO_2$  NPs (not hybridized with GO) showed poor fluoride removal of only 13.4% compared to 85% with  $GO\text{-}CeO_2$  which indicates that GO might have played a major role in achieving the ~72% increase in fluoride removal (Fig. 2a). While effective dispersion of the  $CeO_2$  NPs on the GO sheets (See TEM micrograph in Fig. 1a) possibly helped in enhanced fluoride removal, the  $GO\text{-}CeO_2$  hybrid configuration might have also played additional roles. It is also worth noting that we used a dose of 1 g/L of  $CeO_2$  NPs and  $GO\text{-}CeO_2$  where the amount (mass) of  $CeO_2$  was not the same (while  $CeO_2$  was pure,  $GO\text{-}CeO_2$  was a hybrid of GO and  $CeO_2$  and 1 g of the nanohybrid contained less than 1 g of  $CeO_2$ ). The role of GO is worth investigating.

When an oxygen vacancy is created in  $CeO_2$  NPs, two electrons are released and left at the vacancy site of  $CeO_2$  NPs, and these electrons remain localized in the f level of two cerium atoms and eventually help to reduce  $Ce^{4+}$  to  $Ce^{3+}$  (Joung et al., 2011; Pirmohamed et al., 2010; Skorodumova et al., 2002). GO sheets have both mobile holes and mobile electrons (Yeh et al., 2013). When  $CeO_2$  nanoparticles are decorated onto GO sheets (in  $GO-CeO_2$ ), the electrons in  $CeO_2$  (localized in the f

level) interact with the mobile holes of GO sheets via electrostatic interaction (Joung et al., 2011) (Fig. 5c, iii). Therefore, the mobile holes of GO sheets get trapped at the oxygen vacancy sites of  $CeO_2$  NPs, and as a result, the mobile electrons present in GO sheets now face less resistance and can move along the GO sheets easily (Fig. 5c, iii). The mobile electrons present in the GO sheet move to the  $CeO_2$  lattice (in  $GO-CeO_2$ ) and reduce more  $Ce^{4+}$  to  $Ce^{3+}$  at the  $CeO_2$  NPs-GO interface (Wang et al., 2018; Xia et al., 2017) (Fig. 5c, iii). The new  $Ce^{3+}$  also interacts with  $F^-$  ions to form complex, and that creates more oxygen vacancies. The GO sheets in this study might have facilitated the adsorption of fluoride onto  $GO-CeO_2$  by serving as an effective electron carrier. Others also reported electron transfer between metal oxide nanoparticles and GO sheets while reporting aqueous arsenic (Das et al., 2020) and methylene blue (Mohamadi and Ghorbanali, 2020) removal by other types of GO-based nanohybrids.

Our claim that GO was playing a major role in achieving high fluoride removal needed additional validation by ruling out major  $CeO_2$  NP surface area impact on fluoride removal. We conducted two sets of experiments (details in SI, Section S2.7) with only  $CeO_2$  NPs (no GO) where we sonicated the nanoparticles in one experiment (SI, Fig. S6a) and used Tween 20 surfactant (SI, Fig. S6b) in another to disperse the nanoparticles. Increased dispersion (reduced agglomeration) enhanced

the removal performance slightly (from 9% to 12% with sonication and 9% to 25% with Tween 20) but did not match the removal performance of GO-CeO $_2$  (85%). These results indicate that the reactive surface area is not the only factor that playing a role in the increase of fluoride removal efficiency. While the dispersion of CeO $_2$  NPs in the GO sheet reduces nanoparticle agglomeration to make them more reactive, the GO-CeO $_2$  hybrid configuration drastically enhances the reactivity of the ceria by possibly mediating an electron transfer process between the GO sheet and ceria.

#### 3.4. Environmental application

The synthesis of graphene oxide ceria nanohybrid (GO-CeO<sub>2</sub>) is a simple and scalable process. The fluoride removal capacity of GO-CeO<sub>2</sub> is comparable or better than commercially available adsorbents (SI, Table S1). GO-CeO<sub>2</sub> is effective in a wide range of pH (4-10) (Fig. 3a) and the inferences by coexisting ions are comparable to the commercially available adsorbents (SI, Table S3), GO-CeO<sub>2</sub> can potentially be used for point-of-use and community treatment units. Assuming 5 mg/L raw water fluoride and a 1.5 mg F<sup>-</sup>/L limit as per WHO guidelines, we calculated the amount of GO-CeO<sub>2</sub> needed for a household treatment unit (filter) to treat 30 L of water per family per day and compared that with two conventional fluoride adsorbents (detailed calculations in SI, Section S2.8, and Table S3). If the unit is run in near-neutral pH, 4.45 kg of GO-CeO<sub>2</sub> will be needed per year, but the running unit with adjusted raw water pH of 4 would reduce the amount to 2.38 kg per year. Further, minimal desorption of the adsorbed fluoride from the used GO-CeO<sub>2</sub> (Fig. 3e) makes it even more attractive. Before any field application, further studies are needed to optimize the material performance under continuous flow conditions and with actual F<sup>-</sup> contaminated groundwater. In addition, the leaching of metal (cerium) ions in the effluent should be investigated before field applications.

#### 4. Conclusions

This study has evaluated the performance of a GO-CeO<sub>2</sub> nanohybrid for the fast capture of fluoride from water and investigated the mechanisms involved. The GO-CeO<sub>2</sub> nanohybrid exhibited ultra-rapid kinetics for fluoride removal by reaching the equilibrium within 1 min which is at least 40 times faster than other ceria-based materials reported for fluoride removal and at least 20 times faster than all other materials reported including typical aluminum-based adsorbents. The adsorption capacity of GO-CeO<sub>2</sub> was found to be 8.61 mg/g. The GO-CeO<sub>2</sub> exhibited effective fluoride removal over a wide range of pH (4-10). This novel material contains highly effective  $Ce^{3+}-O^{2-}$  in the lattice which plays a major role in the fast capture of aqueous fluoride via ion exchange. The GO sheet facilitated the fluoride removal process by serving as an effective electron mediator to reduce Ce<sup>4+</sup> to Ce<sup>3+</sup>, and Ce<sup>3+</sup> continuously adsorbed more fluoride to make an insoluble complex. Because of its extremely rapid kinetics, the nanohybrid has the potential for use in high throughput defluoridation systems. To the best of our knowledge, this is the first time that fluoride removal by GO-CeO<sub>2</sub> nanohybrid and the possible mechanisms involved are reported.

#### **CRediT authorship contribution statement**

**Umma S. Rashid:** Conceptualization, Methodology, Data curation, Formal analysis, Visualization, Writing – original draft, Investigation. **Tonoy K. Das:** Conceptualization, Methodology, Data curation, Formal analysis, Visualization, Writing – original draft, Investigation. **Tamil S. Sakthivel:** Resources, Data curation, Visualization, Formal analysis, Investigation, Writing – review & editing. **Sudipta Seal:** Supervision, Resources, Validation, Writing – review & editing, Project administration, Funding acquisition. **Achintya N. Bezbaruah:** Supervision, Resources, Validation, Writing – review & editing, Project administration, Funding acquisition.

#### **Declaration of competing interest**

The authors declare that they have no known competing financial interests or personal relationships that could have appeared to influence the work reported in this paper.

#### Acknowledgments

This work was funded by NSF (Grant# CBET-1707093, PI: Bezbaruah). Rashid and Das received a fellowship from North Dakota Water Resources Research Institute (NDWRRI). Das also received fellowships from the Indian Council of Agricultural Research and NDWRRI. Sudipta Seal acknowledges the NSF MRI grant for XPS (Grant# ECCS-1726636).

# Appendix A. Supplementary information

Supplementary information to this article can be found online at https://doi.org/10.1016/j.scitotenv.2021.148547.

#### References

- Ahmad, S., Gopalaiah, K., Chandrudu, S.N., Nagarajan, R., 2014. Anion (fluoride)-doped ceria Nanocrystals: synthesis, characterization, and its catalytic application to oxidative coupling of benzylamines. Inorg. Chem. 53, 2030–2039.
- Amini, M., Mueller, K., Abbaspour, K.C., Rosenberg, T., Afyuni, M., Moller, K.N., et al., 2008. Statistical modeling of global geogenic fluoride contamination in groundwaters. Environ. Sci. Technol. 42, 3662–3668.
- Araga, R., Sharma, C.S., 2017. Adsorption of fluoride in aqueous solution using Jamun (Syzygium cumini) seed derived activated carbon. Abstr. Pap. Am. Chem. Soc. 253.
- Araga, R., Soni, S., Sharma, C.S., 2017. Fluoride adsorption from aqueous solution using activated carbon obtained from KOH-treated jamun (*Syzygium cumini*) seed. J. Environ. Chem. Eng. 5, 5608–5616.
- Banerjee, A., 2015. Groundwater fluoride contamination: a reappraisal. Geosci. Front. 6, 277–284.
- Bhagawan, D., Saritha, P., Shankaraiah, G., Himabindu, V., 2019. Fluoride removal from groundwater using hybrid cylindrical electrocoagulation reactor. J. Water Chem. Technol. 41 (3), 164–169.
- Bhatnagar, A., Kumar, E., Sillanpaa, M., 2011. Fluoride removal from water by adsorption-a review. Chem. Eng. J. 171, 811–840.
- Campbell, C.T., Peden, C.H.F., 2005. Chemistry oxygen vacancies and catalysis on ceria surfaces. Science 309, 713–714.
- Cao, Z., Li, H., Lowry, G.V., Shi, X., Pan, X., Xu, X., Henkelman, G., Xu, J., 2021. Unveiling the role of sulfur in rapid defluorination of florfenicol by sulfidized nanoscale zero-valent iron in water under ambient conditions. Environ. Sci. Technol. 55, 2628–2638.
- Chai, L.Y., Wang, Y.Y., Zhao, N., Yang, W.C., You, X.Y., 2013. Sulfate-doped Fe3O4/Al2O3 nanoparticles as a novel adsorbent for fluoride removal from drinking water. Water Res. 47, 4040–4049.
- Chen, L., Zhang, K.S., He, J.Y., Cai, X.G., Xu, W.H., Liu, J.H., 2016a. Performance and mechanism of hierarchically porous Ce-Zr oxide nanospheres encapsulated calcium alginate beads for fluoride removal from water. RSC Adv. 6, 36296–36306.
- Chen, L., Zhang, K.S., He, J.Y., Xu, W.H., Huang, X.J., Liu, J.H., 2016b. Enhanced fluoride removal from water by sulfate-doped hydroxyapatite hierarchical hollow microspheres. Chem. Eng. J. 285, 616–624.
- Chen, C.L., Park, S.W., Huang, C.P., 2017. Functionalized activated carbons for enhancing fluoride removal capacity from water. Abstr. Pap. Am. Chem. Soc. 254.
- Chi, Y., Chen, Y., Hu, C., Wang, Y., Liu, C., 2017. Preparation of Mg-Al-Ce triple-metal composites for fluoride removal from aqueous solutions. J. Mol. Liq. 242, 416–422.
- Chigondo, M., Paumo, H.K., Bhaumik, M., Pillay, K., Maity, A., 2018a. Hydrous CeO<sub>2</sub>-Fe<sub>3</sub>O<sub>4</sub> decorated polyaniline fibers nanocomposite for effective defluoridation of drinking water. J. Colloid Interface Sci. 532, 500–516.
- Chigondo, M., Paumo, H.K., Bhaumik, M., Pillay, K., Maity, A., 2018b. Rapid high adsorption performance of hydrous cerium-magnesium oxides for removal of fluoride from water. J. Mol. Liq. 265, 496–509.
- Chouhan, S., Flora, S.J.S., 2010. Arsenic and fluoride: two major ground water pollutants. Indian J. Exp. Biol. 48, 666–678.
- Das, T.K., Sakthivel, T.S., Jeyaranjan, A., Seal, S., Bezbaruah, A.N., 2020. Ultra-high arsenic adsorption by graphene oxide iron nanohybrid: removal mechanisms and potential applications. Chemosphere 253.
- Dash, S.S., Sahu, M.K., Sahu, E., Patel, R.K., 2015. Fluoride removal from aqueous solutions using cerium loaded mesoporous zirconium phosphate. New J. Chem. 39, 7300–7308.
- Deng, S.B., Liu, H., Zhou, W., Huang, J., Yu, G., 2011. Mn-Ce oxide as a high-capacity adsorbent for fluoride removal from water. J. Hazard. Mater. 186, 1360–1366.
- Dhillon, A., Sharma, T.K., Soni, S.K., Kumar, D., 2016. Fluoride adsorption on a cubical ceria nanoadsorbent: function of surface properties. RSC Adv. 6, 89198–89209.
- Di, Z.C., Li, Y.H., Peng, X.J., Luan, Z.K., Liang, J., 2007. Adsorption of fluoride by aligned carbon nanotubes supported ceria nanoparticles. Solid State Phenom. 121–123, 1221–1224.
- Dutta, P., Pal, S., Seehra, M.S., Shi, Y., Eyring, E.M., Ernst, R.D., 2006. Concentration of Ce<sup>3+</sup> and oxygen vacancies in cerium oxide nanoparticles. Chem. Mater. 18, 5144–5146.

- Gbadebo, A.M., 2012. Groundwater fluoride and dental fluorosis in southwestern Nigeria. Environ. Geochem. Health 34, 597–604.
- George, S., Pandit, P., Gupta, A.B., 2010. Residual aluminium in water defluoridated using activated alumina adsorption modeling and simulation studies. Water Res. 44, 3055–3064
- Ghorai, S., Pant, K.K., 2005. Equilibrium, kinetics and breakthrough studies for adsorption of fluoride on activated alumina. Sep. Purif. Technol. 42, 265–271.
- Goswami, A., Purkait, M.K., 2012. The defluoridation of water by acidic alumina. Chem. Eng. Res. Des. 90, 2316–2324.
- Hayes, K.F., Papelis, C., Leckie, J.O., 1988. Modeling ionic-strength effects on anion adsorption at hydrous oxide solution interfaces. J. Colloid Interface Sci. 125, 717–726.
- International Organization for Standardization(ISO), ISO BS 14887, 2000. Sample Preparation-Dispersing Procedures for Powders in Liquids. International Organization for Standardization, Geneva, Switzerland.
- Jagtap, S., Yenkie, M.K., Labhsetwar, N., Rayalus, S., 2012. Fluoride in drinking water and defluoridation of water. Chem. Rev. 112, 2454–2466.
- Joung, D., Singh, V., Park, S., Schulte, A., Seal, S., Khondaker, S.I., 2011. Anchoring ceria nanoparticles on reduced graphene oxide and their electronic transport properties. J. Phys. Chem. C 115, 24494–24500.
- Kang, D., Yu, X., Ge, M., 2017. Morphology-dependent properties and adsorption performance of CeO<sub>2</sub> for fluoride removal. Chem. Eng. J. 330, 36–43.
- Karmakar, S., Dechnik, J., Janiak, C., De, S., 2016. Aluminium fumarate metal-organic framework: a super adsorbent for fluoride from water. J. Hazard. Mater. 303, 10–20.
- Kovtun, A., Treossi, E., Mirotta, N., Scida, A., Liscio, A., Christian, M., et al., 2019. Benchmarking of graphene-based materials: real commercial products versus ideal graphene. 2D Mater. 6, 025006.
- Kuang, L.Y., Liu, Y.Y., Fu, D.D., Zhao, Y.P., 2017. FeOOH-graphene oxide nanocomposites for fluoride removal from water: acetate mediated nano FeOOH growth and adsorption mechanism. J. Colloid Interface Sci. 490, 259–269.
- Kumar, A., Babu, S., Karakoti, A.S., Schulte, A., Seal, S., 2009. Luminescence properties of europium-doped cerium oxide nanoparticles: role of vacancy and oxidation states. Langmuir 25, 10998–11007.
- Li, Z.J., Deng, S.B., Zhang, X.Y., Zhou, W., Huang, J., Yu, G., 2010. Removal of fluoride from water using titanium-based adsorbents. Front. Environ. Sci. Eng. China 4, 414–420.
- Liu, C.H., Chuang, Y.H., Chen, T.Y., Tian, Y., Li, H., Wang, M.K., et al., 2015. Mechanism of arsenic adsorption on magnetite nanoparticles from water: thermodynamic and spectroscopic studies. Environ. Sci. Technol. 49, 7726–7734.
- Liu, L., Cui, Z.J., Ma, Q.C., Cui, W., Zhang, X., 2016. One-step synthesis of magnetic ironaluminum oxide/graphene oxide nanoparticles as a selective adsorbent for fluoride removal from aqueous solution. RSC Adv. 6, 10783–10791.
- Lv, L., He, J., Wei, M., Evans, D.G., Zhou, Z.L., 2007. Treatment of high fluoride concentration water by MgAl-CO3 layered double hydroxides: kinetic and equilibrium studies. Water Res. 41, 1534–1542.
- Martyn, C.N., Osmond, C., Edwardson, J.A., DJP, Barker, Harris, E.C., Lacey, R.F., 1989. Geographical relation between alzheimers-disease and aluminum in drinking-water. Lancet 1, 59–62.
- McCormack, R.N., Mendez, P., Barkam, S., Neal, C.J., Das, S., Seal, S., 2014. Inhibition of nanoceria's catalytic activity due to Ce<sup>3+</sup> site-specific interaction with phosphate ions. J. Phys. Chem. C 118, 18992–19006.
- Meenakshi, Maheshwari, R.C., 2006. Fluoride in drinking water and its removal. J. Hazard. Mater. 137, 456–463.
- Menon, M.P., James, J., Jackson, J.D., 1986. Complexation, solubilities and thermodynamic functions for cerium(iii) fluoride-water system. J. Radioanal. Nucl. Chem. 102, 419–428.
- Mkhoyan, K.A., Contryman, A.W., Silcox, J., Stewart, D.A., Eda, G., Mattevi, C., et al., 2009. Atomic and electronic structure of graphene-oxide. Nano Lett. 9, 1058–1063.
- Mohamadi, S., Ghorbanali, M., 2020. Adsorption and UV-assisted photodegradation of methylene blue by CeO<sub>2</sub>-decorated graphene sponge. Sep. Sci. Technol. 1–11.
- Mohan, S., Kumar, V., Singh, D.K., Hasan, S.H., 2016. Synthesis and characterization of rGO/ZrO<sub>2</sub> nanocomposite for enhanced removal of fluoride from water: kinetics, isotherm, and thermodynamic modeling and its adsorption mechanism. RSC Adv. 6, 87523–87538.
- Mohanty, K., Jha, M., Meikap, B.C., Biswas, M.N., 2005. Removal of chromium(VI) from dilute aqueous solutions by activated carbon developed from Terminalia arjuna nuts activated with zinc chloride. Chem. Eng. Sci. 60, 3049–3059.
- Mohapatra, M., Anand, S., Mishra, B.K., Giles, D.E., Singh, P., 2009. Review of fluoride removal from drinking water. J. Environ. Manag. 91, 67–77.
- Mukhopadhyay, K., Ghosh, A., Das, S.K., Show, B., Sasikumar, P., Ghosh, U.C., 2017. Synthesis and characterisation of cerium(IV)-incorporated hydrous iron(III) oxide as an adsorbent for fluoride removal from water. RSC Adv. 7, 26037–26051.
- Narsimha, A., Sudarshan, V., 2017. Contamination of fluoride in groundwater and its effect on human health: a case study in hard rock aquifers of Siddipet, Telangana State, India. Appl Water Sci 7, 2501–2512.
- Perreault, F., de Faria, A.F., Elimelech, M., 2015. Environmental applications of graphenebased nanomaterials. Chem. Soc. Rev. 44, 5861–5896.
- Pirmohamed, T., Dowding, J.M., Singh, S., Wasserman, B., Heckert, E., Karakoti, A.S., et al., 2010. Nanoceria exhibit redox state-dependent catalase mimetic activity. Chem. Commun. 46, 2736–2738.
- Rashid, U.S., Bezbaruah, A.N., 2020. Citric acid modified granular activated carbon for enhanced defluoridation. Chemosphere 252.
- Rohder, L.A., Brandt, T., Sigg, L., Behra, R., 2014. Influence of agglomeration of cerium oxide nanoparticles and speciation of cerium(III) on short term effects to the green algae Chlamydomonas reinhardtii. Aquat. Toxicol. 152, 121–130.
- Ruan, Z.Y., Tian, Y.X., Ruan, J.F., Cui, G.J., Iqbal, K., Iqbal, A., et al., 2017. Synthesis of hydroxyapatite/multi-walled carbon nanotubes for the removal of fluoride ions from solution. Appl. Surf. Sci. 412, 578–590.

- Sadeghi, M.H., Tofighy, M.A., Mohammadi, T., 2020. One-dimensional graphene for efficient aqueous heavy metal adsorption: rapid removal of arsenic and mercury ions by graphene oxide nanoribbons (GONRs). Chemosphere 253.
- Safi, M., Sarrouj, H., Sandre, O., Mignet, N., Berret, J.F., 2010. Interactions between sub-10-nm iron and cerium oxide nanoparticles and 3T3 fibroblasts: the role of the coating and aggregation state. Nanotechnology 21.
- Sakthivel, T.S., Das, S., Pratt, C.J., Seal, S., 2017. One-pot synthesis of a ceria-graphene oxide composite for the efficient removal of arsenic species. Nanoscale 9, 3367–3374
- Sayle, T.X., Caddeo, F., Zhang, X., Sakthivel, T., Das, S., Seal, S., Ptasinska, S., Sayle, D.C., 2016. Structure–activity map of ceria nanoparticles, nanocubes, and mesoporous architectures. Chem. Mater. 28 (20), 7287–7295.
- Schmitt, R., Nenning, A., Kraynis, O., Korobko, R., Frenkel, A.I., Lubomirsky, I., et al., 2020. A review of defect structure and chemistry in ceria and its solid solutions. Chem. Soc. Rev. 49, 554–592.
- Seal, S., Jeyaranjan, A., Neal, C.J., Kumar, U., Sakthivel, T.S., Sayle, D.C., 2020. Engineered defects in cerium oxides: tuning chemical reactivity for biomedical, environmental, & energy applications. Nanoscale 12, 6879–6899.
- Sharma, R., Raghav, S., Nair, M., Kumar, D., 2018. Kinetics and adsorption studies of mercury and lead by ceria nanoparticles entrapped in tamarind powder. ACS Omega 3, 14606–14619.
- Skorodumova, N.V., Simak, S.I., Lundqvist, B.I., Abrikosov, I.A., Johansson, B., 2002. Quantum origin of the oxygen storage capability of ceria. Phys. Rev. Lett. 89.
- Slater, J.C., 1964. Atomic radii in crystals. J. Chem. Phys. 41, 3199-3204.
- Strunecka, A., Patocka, J., 1999. Pharmacological and toxicological effects of aluminofluoride complexes. Fluoride 32, 230–242.
- Sujana, M.G., Thakur, R.S., Rao, S.B., 1998. Removal of fluoride from aqueous solution by using alum sludge. J. Colloid Interface Sci. 206, 94–101.
- Tang, D., Zhang, G., 2016. Efficient removal of fluoride by hierarchical Ce-Fe bimetal oxides adsorbent: thermodynamics, kinetics and mechanism. Chem. Eng. J. 283, 721–729.
- Thakur, L.S., Mondar, P., 2017. Simultaneous arsenic and fluoride removal from synthetic and real groundwater by electrocoagulation process: parametric and cost evaluation. J. Environ. Manag. 190, 102–112.
- United States Environmental Protection Agency (USEPA), 2009. National primary drinking water regulations. Available:. https://www.epa.gov/ground-water-and-drinking-water/national-primary-drinking-water-regulations#Inorganic. (Accessed 25 February 2021).
- Valicsek, Z., Kovacs, M., Horvath, O., 2019. Explanation for the multi-component scintillation of cerium fluoride through the equilibrium and photophysical investigation of cerium(III)-Fluoro complexes. Nanomaterials 9.
- Wang, J., Xu, W.H., Chen, L., Jia, Y., Wang, L., Huang, X.J., et al., 2013. Excellent fluoride removal performance by CeO<sub>2</sub>-ZrO<sub>2</sub> nanocages in water environment. Chem. Eng. J. 231, 198–205.
- Wang, H., Feng, Q.M., Liu, K., Li, Z.S., Tang, X.K., Li, G.Z., 2017. Highly efficient fluoride adsorption from aqueous solution by nepheline prepared from kaolinite through alkalihydrothermal process. J. Environ. Manag. 196, 72–79.
- Wang, Z.Q., Zhao, P.F., He, D.N., Cheng, Y., Liao, L.S., Li, S.D., et al., 2018. Cerium oxide immobilized reduced graphene oxide hybrids with excellent microwave absorbing performance. Phys. Chem. Chem. Phys. 20, 14155–14165.
- Weber, W.J., Morris, J.C., 1963. Kinetics of adsorption on carbon from solution. J. Sanit. Eng. Div. 89, 31–60.
- Wendt, S., Matthiesen, J., Schaub, R., Vestergaard, E.K., Laegsgaard, E., Besenbacher, F., et al., 2006. Formation and splitting of paired hydroxyl groups on reduced TiO<sub>2</sub>(110). Phys. Rev. Lett. 96.
- World Health Organization (WHO), 2004. Guidelines for Drinking-water Quality. 3rd ed. vol. 1. World Health Organization, Geneva (recommendations).
- Wu, Z.S., Yang, S.B., Sun, Y., Parvez, K., Feng, X.L., Mullen, K., 2012. 3D nitrogen-doped graphene aerogel-supported Fe<sub>3</sub>O<sub>4</sub> nanoparticles as efficient eletrocatalysts for the oxygen reduction reaction. J. Am. Chem. Soc. 134, 9082–9085.
- Xia, W., Zhao, J., Wang, T., Song, L., Gong, H., Guo, H., et al., 2017. Anchoring ceria nanoparticles on graphene oxide and their radical scavenge properties under gamma irradiation environment. Phys. Chem. Chem. Phys. 19, 16785–16794.
- Xiao, H., Ai, Z., Zhang, L., 2009. Nonaqueous sol-gel synthesized hierarchical CeO<sub>2</sub> nanocrystal microspheres as novel adsorbents for wastewater treatment. J. Phys. Chem. C 113, 16625–16630.
- Yadav, K.K., Gupta, N., Kumar, V., Khan, S.A., Kumar, A., 2018. A review of emerging adsorbents and current demand for defluoridation of water: bright future in water sustainability. Environ. Int. 111, 80–108.
- Yeh, T.F., Cihlar, J., Chang, C.Y., Cheng, C., Teng, H.S., 2013. Roles of graphene oxide in photocatalytic water splitting. Mater. Today 16, 78–84.
- Yu, X.F., Liu, J.W., Cong, H.P., Xue, L., Arshad, M.N., Albar, H.A., et al., 2015. Templateand surfactant-free synthesis of ultrathin CeO<sub>2</sub> nanowires in a mixed solvent and their superior adsorption capability for water treatment. Chem. Sci. 6, 2511–2515.
- Yu, Z.C., Xu, C.H., Yuan, K.K., Gan, X.Z., Feng, C., Wang, X.Q., et al., 2018. Characterization and adsorption mechanism of ZrO<sub>2</sub> mesoporous fibers for health-hazardous fluoride removal. J. Hazard. Mater. 346, 82–92.
- Zhang, F., Chan, S.W., Spanier, J.E., Apak, E., Jin, Q., Robinson, R.D., et al., 2002. Cerium oxide nanoparticles: size-selective formation and structure analysis. Appl. Phys. Lett. 80, 127–129.
- Zhang, J., Chen, N., Su, P.Y., Li, M., Feng, C.P., 2017. Fluoride removal from aqueous solution by zirconium-chitosan/graphene oxide membrane. React. Funct. Polym. 114, 127–135.

- Zhang, J., Kong, Y.Q., Yang, Y., Chen, N., Feng, C.P., Huang, X.D., et al., 2019a. Fast capture of fluoride by anion-exchange zirconium-graphene hybrid adsorbent. Langmuir 35, 6861–6869.
- Zhang, Y.Y., Qian, Y., Li, W., Gao, X., Pan, B., 2019b. Fluoride uptake by three lanthanum based nanomaterials: behavior and mechanism dependent upon lanthanum species. Sci. Total Environ. 683, 609–616.
- Zhang, S., Wang, H., Liu, J., Bao, C., 2020. Measuring the specific surface area of monolayer graphene oxide in water. Mater. Lett. 261.
  Zhao, X.L., Wang, J.M., Wu, F.C., Wang, T., Cai, Y.Q., Shi, Y.L., et al., 2010. Removal of fluoride from aqueous media by Fe<sub>3</sub>O<sub>4</sub>@Al(OH)<sub>3</sub> magnetic nanoparticles. J. Hazard. Mater. 173, 102–109.